Room-temperature reaction of laser-photolytically generated Te nanosols with silver

Akihiko Ouchi [a,*], Zdeněk Bastl [b], Jaroslav Boháček [c], Jan Šubrt [c], Snejana Bakardjieva [c], Petr Bezdička [c], Josef Pola [d,**]

[a] National Institute of Advanced Industrial Science and Technology, AIST, Tsukuba, Ibaraki 305-8565, Japan
[b] J. Heyrovský Institute of Physical Chemistry, ASCR, 18223 Prague, Czech Republic
[c] Institute of Inorganic Chemistry, ASCR, 25068 Řež, Czech Republic
[d] Laboratory of Laser Chemistry, Institute of Chemical Process Fundamentals, ASCR, 16502 Prague, Czech Republic

ARTICLE INFO

ABSTRACT

KrF laser photolysis of diphenyl ditelluride in 2-propanol yields a stable solution of tellurium nanosols, which reacts with immersed Ag sheets to yield thin silver telluride films. The nanosols were identified by UV–vis spectroscopy and the films were characterized by electron microscopy, X-ray photoelectron spectroscopy and X-ray diffraction analysis. It is revealed that the films are mostly amorphous and contain small contributions of cubic as well as monoclinic Ag_2Te structures. The procedure provides the first example of the fast formation of silver telluride thin films by reaction between the elements in inert solvent at room-temperature.

1. Introduction

Silver telluride Ag_2Te has been given much attention due to its interesting polymorphism [1–4], ionic superconductivity, semiconducting properties [5,6] and giant magnetoresistence [7,8] all of which suggest more research in and wide application of this compound in future. One of the challenges is fabrication of new thin films and nanosized objects that can find use in microelectronics, thermoelectronics and magnetics.

Bulk Ag_2Te was conventionally obtained by solid-state reaction between Ag and Te at very high-temperatures [9] or by rather slow room-temperature reaction between Ag and Te in *n*-butylamine [10].

Recent development of nanoscience spurred further interest in synthesis of Ag_2Te thin films and nanosized features by using various methods. Thus, nanowires were obtained by electrodeposition from $AgNO_3$–$TeCl_4$ dimethyl sulfoxide solutions [11] and nanocrystals were prepared by sonochemical synthesis from $AgNO_3$–Te [12] and AgCl–Te [13] ethylenediamine solutions, as well as by sono-

chemical polyol reduction method [14]. Size-tunable nanocrystals were recently prepared using $AgNO_3$ and trioctylphosphine-tellurium complex [15]. Nanofibers were obtained from aqueous solution of Te fibers and $AgNO_3$ [16].

Nanostructured films were prepared through reaction of $AgNO_3$ and trioctylphosphine-tellurium complex [15], electrodeposited from $AgNO_3$–$TeCl_4$ dimethyl sulfoxide solutions [17], hydrothermally grown through reaction between Ag foil and Te powder [18] and developed through solid-state reaction of Ag and Te thin film couples [19,20]. In the last simple approach, Ag_2Te films grown at room-temperature consisted of monoclinic and orthorhombic phase [20] and those grown at elevated temperature (below 200 °C) were composed of monoclinic phase and polycrystalline features [19].

We have previously reported on UV and IR laser-induced gas-phase photolysis of several organotellurium compounds for chemical vapor [21–24] and liquid [25] deposition of nanostructured tellurium films. Our further interest was in room-temperature reaction between metal surfaces and selenium films laser-photolytically deposited on these surfaces [26].

In conjunction with these studies, we now report that laser photolysis of organotellurium compound (diphenyl ditelluride) in inert organic solvent results in the formation of Te nanosols which react with immersed Ag surface to yield Ag_2Te films. We show that

* Corresponding author. Tel.: +81 298614550; fax: +81 298614421.
** Corresponding author. Tel.: +420 220390308; fax: +420 220920661.
E-mail addresses: ouchi.akihiko@aist.go.jp (A. Ouchi), pola@icpf.cas.cz (J. Pola).

this one-step and room-temperature procedure represents a convenient and fast approach to amorphous Ag_2Te films containing very small contributions of crystalline structures.

2. Experimental

Diphenyl ditelluride (98%, Aldrich) solution (10^{-3} M, 30 ml) in 2-propanol, hexane (both Cica-reagent for spectroscopy, Kanto), or diethyl ether (dry, Wako) was placed in a quartz tube (3 cm in diameter, 10 cm long) equipped with a valve for connection to a vacuum line. The solutions were de-aerated (three vacuum freeze–thaw cycles), bubbled with Ar and then stirred by a magnetic bar and irradiated under Ar with an LPX-200 (Lambda Physik) laser. The KrF laser radiation at 248 nm with a repetition frequency of 5 Hz delivering energy of 480 mJ per pulse (measured by a Gentec ED-500 joulmeter) was mildly focused to incident area of 1.8 cm^2. The solutions were irradiated for 3 min, which corresponded to spectral changes given in Fig. 1. During this time they developed dark brown color. The photolytic progress was monitored on the aliquots (0.4 ml) withdrawn from the irradiated solution and diluted with the corresponding solvent (3.6 ml) by UV–vis spectrometry (a Shimadzu UV-2450 UV–vis spectrometer) in the 4 ml quartz cells.

The photolyzed solutions were left to stay until they developed black sediment which was centrifuged and washed with hexane. The sediment suspended in 2-propanol and ultrasonicated for several hours was analyzed by UV spectroscopy (an UV 1601 Shimadzu spectrophotometer). Alternatively, metal (Ag, Cd, Zn, Al, Cu) sheets (area of ca. 0.6 cm^2, 99.99% pure, Soekawa Chemicals) were immersed into freshly photolyzed 2-propanol solutions and left overnight. Thereafter, the sheets were analyzed by X-ray photoelectron spectroscopy, electron microscopy and X-ray diffraction analysis.

The X-ray photoelectron spectra were measured with a Gammadata Scienta ESCA 310 electron spectrometer using monochromatized Al Kα ($h\alpha$ = 1486.6 eV) radiation for electron excitation. The high-resolution spectra of Ag $3d_{5/2}$, (and also of Al 2p, Cu $2p_{3/2}$, Zn $2p_{3/2}$ and Cd $3d_{5/2}$), Te $3d_{5/2}$, C 1s and O 1s photoelectrons and Te $L_3M_{45}M_{45}$ Auger electron spectra were measured for an as-received sample. Quantification of element concentration ratios was accomplished by correcting the photoelectron peak intensities for their cross-sections [27] and accounting for the dependence 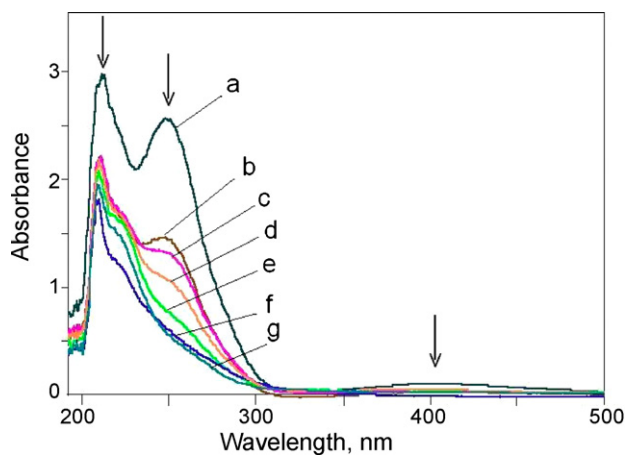of the inelastic mean free path of photoelectrons on their kinetic energy [28]. Curve fitting of overlapping lines was carried out using the lines of a gaussian–lorentzian shape. Core level binding energies were determined with an accuracy ±0.2 eV.

The SEM images were acquired using a Philips XL30 CP scanning electron microscope. TEM analysis (particle size and phase analysis) was carried out on a Philips 201 transmission electron microscope. Process diffraction [29] was used to evaluate and compare measured electron diffraction patterns with an XRD diffraction database [30]. HRTEM micrographs were obtained using a JEOL JEM 3010 operating at 300 kV (LaB6 cathode) and equipped with EDS detector (INCA/Oxford). Nickel grid coated with a holey carbon support film was used. The layer was scraped off, dispersed in ethanol and the suspension was treated in ultrasonic bath for 10 min.

Diffraction pattern were collected with a PANalytical X'Pert PRO diffractometer equipped with a conventional X-ray tube (Co Kα radiation, 40 kV, 30 mA, point focus), an X-ray monocapillary with 0.1 mm diameter and a multichannel detector X'Celerator with an anti-scatter shield and Fe-β filter. A sample holder for single crystal XRD meassurement was adopted by adding z-(vertical) axis adjustment (Huber 1005 goniometer head). To suppress the penetration depth and enhance the signal of a thin layer, the angle of the incident beam was fixed to 3°. The diffraction patterns were taken between 6 and 100° 2Θ with the step of 0.0167° and 2100 s counting per step, which corresponds to total counting time of more than 24 h. Qualitative analysis was performed with HighScore software package (PANalytical, Netherlands, version 1.0d), Diffrac-Plus software package (Bruker AXS, Germany, version 8.0) and JCPDS PDF-2 database [31].

3. Results and discussion

Diphenyl ditelluride exhibits absorption bands at 211, 248 and 406 nm and it is perfectly suited for absorption of 248 nm photons of KrF laser. The laser photolysis of yellow diphenyl ditelluride solutions in 2-propanol, hexane, or diethyl ether results in a deep brown darkening and UV–vis spectral changes identical with all the irradiated solutions. For the sake of brevity, only spectral changes for the 2-propanol solution are illustrated (Fig. 1). The observed major depletion at 248 and 406 nm is in keeping with the extraordinary photochemical lability of diorganyl ditellurides ($R_2Te_2 \rightarrow R_2Te + Te$, $R_2Te \rightarrow R–R + Te$) that are excellent precursors of Te [32,33]. The dark colored solutions in 2-propanol remain

Fig. 1. Absorption spectra of diphenyl ditelluride (10^{-3} M solutions in 2-propanol, 10-times diluted in 2-propanol) before and after irradiation with KrF laser. (The bands gradually descending in the course of photolysis (a–g) are designated by arrows and correspond to irradiation with 0, 3, 6, 16, 40, 100 and 200 pulses.)
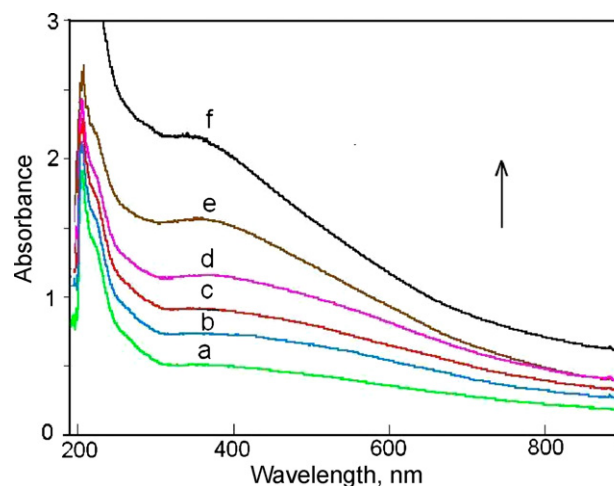

Fig. 2. UV–vis spectrum of black sediment dispersed in 2-propanol in the spectroscopic cell as dependent on time of ultrasonication. (The gradual absorbance growth (a–f) corresponds to 6-fold 1 h ultrasonication.)
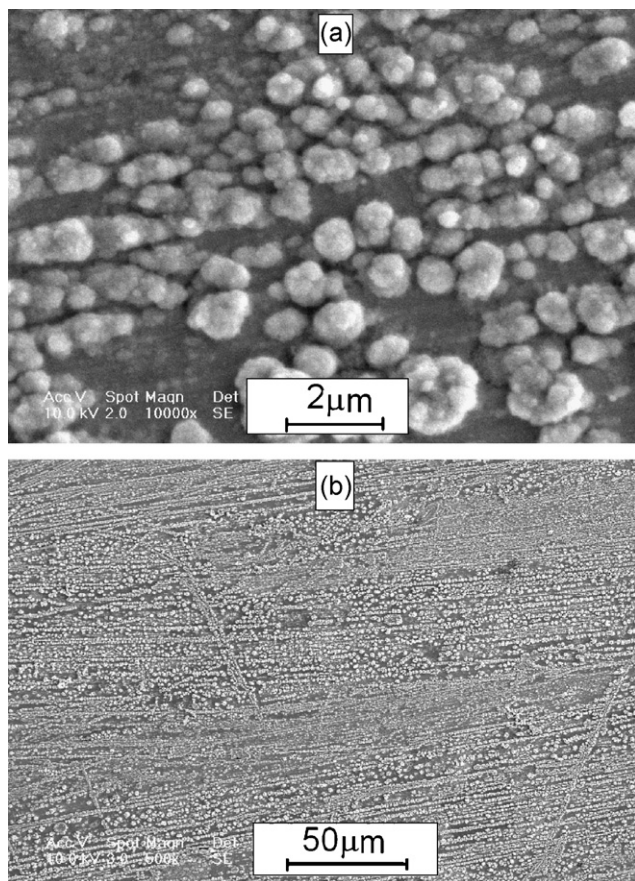
Fig. 3. SEM images of the sediment on Ag sheet.

Fig. 4. EDX–SEM analysis of the sediment on Ag sheet.

transparent and do not form sediment even when refluxed for several hours. The dark solutions in diethyl ether and hexane are less stable. Those in diethyl ether remain black, but become turbid and form a small amount of ultrafine black sediment within less than 1 h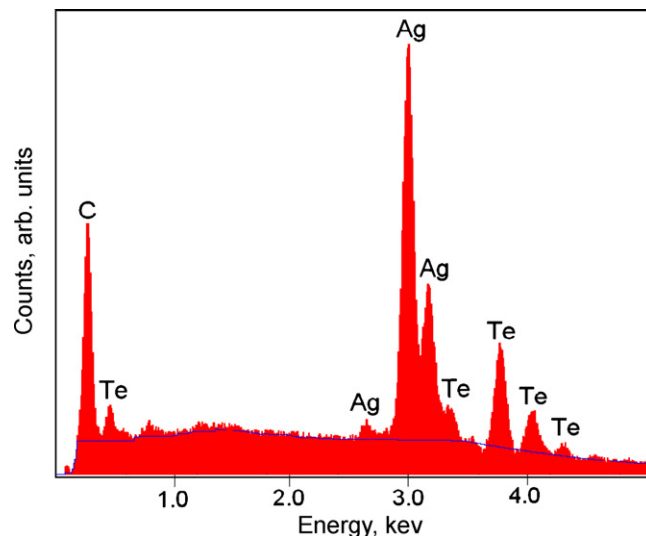. The solutions in hexane, also remaining black, allow a small sedimentation in the form of thin black films adhering to reactor walls even during the photolysis and form substantial amounts of black sediment even within few minutes after the photolysis.

The sediments from hexane solutions dispersed in 2-propanol become transparent, dark brown solution when ultrasonicated for several hours. The UV–vis spectrum of the solution (Fig. 2) shows absorption decaying from 200 nm to higher wavelengths and a broad band centered at ca. 345–380 nm assigned [34] to amorphous Te colloids. We note that absorption around 250 nm is characteristic for Te nanoparticles [35,36]. The decreasing stability of Te nanosols in the selected solvents (2-propanol > diethyl ether > hexane) indicates that Te nanosols are stabilized by polar and hydrophilic groups.

In studying interaction of the photolytically prepared black solutions in 2-propanol with metal (Ag, Cd, Zn, Al, Cu) sheets, we dipped these sheets into the solutions for 48 h. The Ag sheets become dark
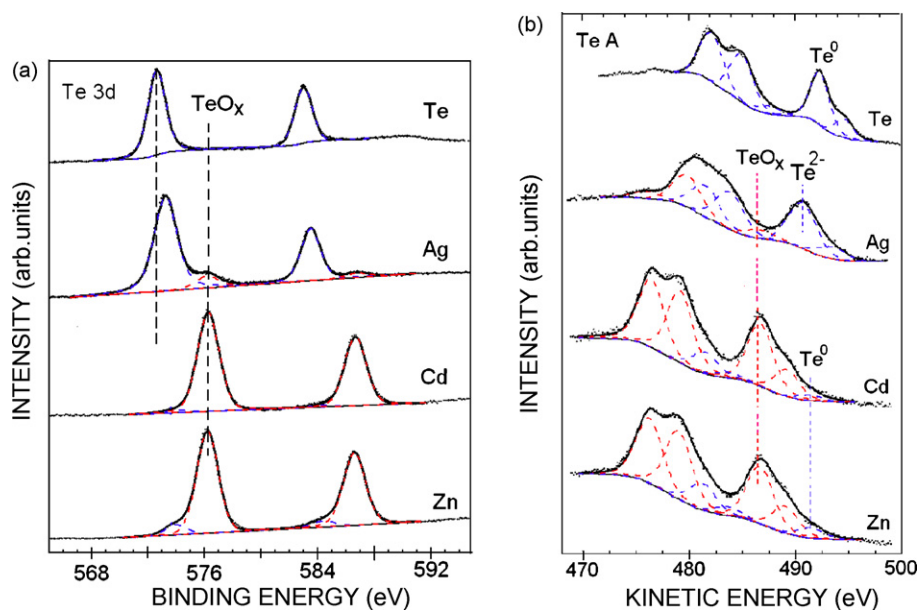

Fig. 5. Spectra of Te 3d core level electrons (a) and Auger Te $L_3M_{45}M_{45}$ spectra (b) of metal sheets and authentic Te sample.
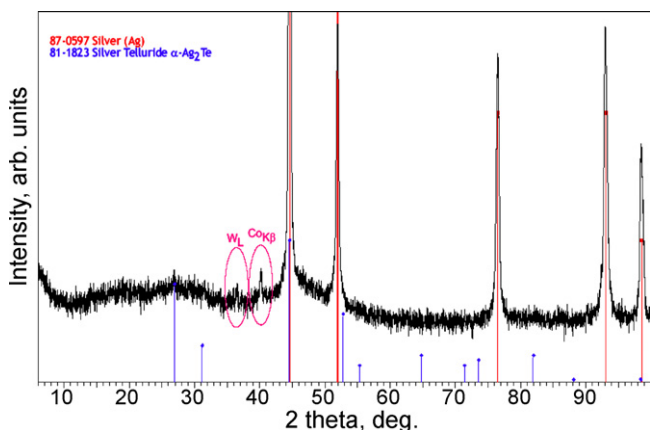
Fig. 6. XRD pattern of Te deposited on Ag sheet (with remaining CO Kβ and W_L lines).

brown in less than 1 h, whereas the other sheets did not change their appearance. The EDX–SEM derived atomic percentage of Te on the Cd, Zn, Al and Cu sheets is 0–2 while that on Ag is 16–20. These numbers indicate a dramatically higher content of Te on Ag. The SEM images of these films reveal ca. 1 μm-sized particles (Fig. 3a) which are arranged in parallel rows (Fig. 3b). This interesting morphology pattern is of theoretical interest. The EDX–SEM derived elemental composition of the 10 μm^2 area of the dark film on the Ag sheet (Fig. 4, $Ag_{1.00}$ $Te_{0.30}$ $C_{0.38}$) and that of the 1 μm^2-sized particle ($Ag_{1.00}$ $Te_{0.45}$ $C_{0.44}$) indicate that the area not covered with the

particles has the same stoichiometry and that the sedimental layer is contaminated by biphenyl.

The XPS analysis of the topmost layers of the dipped metal sheets revealed the presence of the metal and C, Te and O elements. The spectra of Te 3d electrons and $L_3M_{45}M_{45}$ spectra (given only for some metals in Fig. 5) are fully consistent [37,38] with two different states of Te, namely Te^{2-} and TeO_x. On Ag surface Te^{2-} is abundant (90%) and TeO_x is scarce, whereas on the other metals the TeO_x is dominating (91–98%) and Te^{2-} is virtually absent.

The EDX and XPS analyses thus show that Te deposited on Ag reacts with Ag to silver telluride, whereas Te on the other metals (deposited in much lower amounts) undergoes only oxidation.

The X-ray diffraction analysis of the silver telluride film (Fig. 6) is compatible with amorphous phase thickness of which is equal or less than the penetration depth of Co Kα X-rays (0.25 μm at incident angle 3°). The analysis suggests the monoclinic α-Ag_2Te structure in an amount around the detection limit (approximately 2 wt. %).

Further laborious analyses on many agglomerates of the layer confirm the preponderance of amorphous phase and very minor (random) contributions of two different crystalline phases. Thus, the TEM analyses are consistent with a blend of amorphous phase and cubic Ag_2Te structure (Fig. 7), whereas the HRTEM analyses indicate amorphous phase together with the monoclinic Ag_2Te structure (Fig. 8).

The formation of the cubic Ag_2Te structure at room-temperature is not expected, because Ag_2Te exists [1–4] as the low-temperature monoclinic semiconductor and the high-temperature cubic superionic conductor [6] with phase transition at 145 °C.
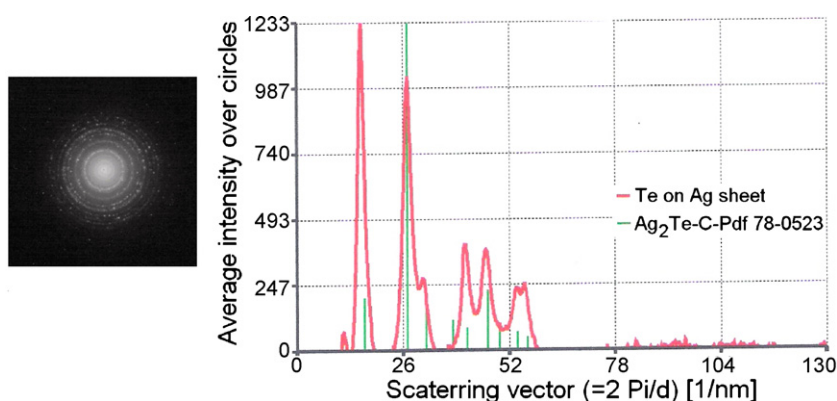

Fig. 7. Electron diffraction of μm-sized particle from Te deposited on Ag sheet revealing cubic Ag_2Te.
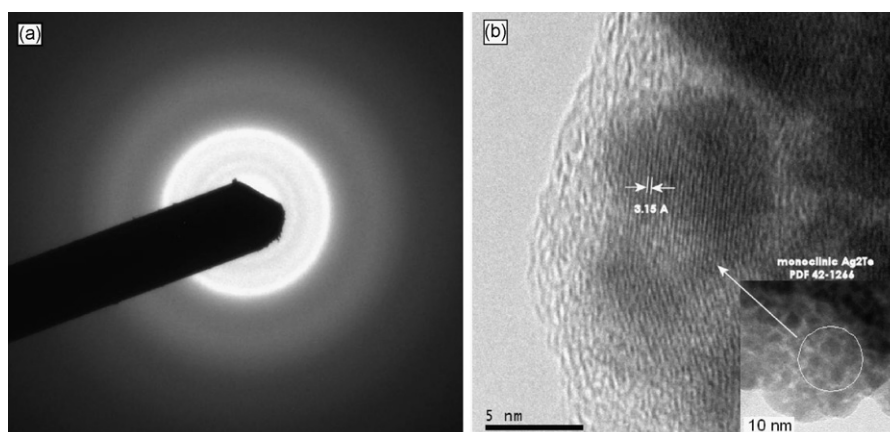

Fig. 8. Electron diffraction, HRTEM image and corresponding SAD pattern of nm-sized body from Te on Ag sheet revealing monoclinic Ag_2Te.

We note that the room-temperature reaction between Ag and Te, leading to cubic superionic conductive structure, was not previously observed and that the solid-state room-temperature reaction between Ag and Te thin film couples gives rise to monoclinic and orthorhombic Ag_2Te structures [20].

In our conditions, Ag_2Te formation occurs through reaction of Ag surface with 2-propanol-stabilized Te nanosols. The primary step of the reaction must be a split of the nanosol solvation shell, an escape of Te nanoparticles and their reaction with Ag surface. The exothermicity of Ag_2Te formation and inter-diffusion of Te and Ag would facilitate the growth of the boundary phase in which crystallization is enhanced after reaching proper Ag/Te ratio. The Te–Ag inter-diffusion was modeled only for elevated temperatures [39]. However, the detection of Ag_2Te in the topmost layers of the sedimental film on Ag sheet by the XPS analysis shows that inter-diffusion is also efficient at room-temperature. Considering that the relative extent of metal and chalcogene inter-diffusion is dependent on cluster size [40], we suggest that Ag–Te inter-diffusion is initially driven by penetration of nanosized Te into Ag and that it is further assisted by chemical diffusion [41] and possibly through the transient formation of the cubic phase through which Ag cations easily move [6]. The reasons for the formation of the cubic structure are not clear at present.

4. Conclusion

KrF laser photolysis of diphenyl ditelluride in 2-propanol, diethyl ether and hexane allows formation of Te colloid solutions. Stability of Te nanosols dramatically decreases with decreasing polarity of the solvent.

Colloidal solutions of tellurium in 2-propanol do not react with Cd, Zn, Al and Cu sheets, but they undergo fast reaction with Ag sheets to yield Ag_2Te thin film. These films show aggregation in continuous parallel rows, are mostly amorphous and contain rare contributions of monoclinic and cubic structures.

The procedure allows a convenient and fast formation of Ag_2Te films on Ag surfaces at room-temperature in inert solvent.

Acknowledgements

References

[1] I. Karakaya, W.T. Thompson, J. Phase Equilib. 12 (1991) 56.
[2] J. Schneider, H. Schulz, Z. Kristallogr. 203 (1993) 1.
[3] C. Manolikas, J. Solid State Chem. 66 (1987) 1–6.
[4] V.D. Das, D. Karunakaran, J. Appl. Phys. 66 (1989) 1822.
[5] W. Gorbachev, Semiconductor Compounds $A^I_2B^{VI}$, Metallurgy, Moscow, 1980.
[6] M. Kobayashi, K. Ishikawa, F. Tachibana, H. Okazaki, Phys. Rev. B 38 (1988) 3050.
[7] R. Xu, A. Husmann, T.F. Rosenbaum, M.-L. Saboungi, J.E. Enderby, P.B. Littlewood, Nature 390 (1997) 57.
[8] I.S. Chuprakov, K.H. Dahmen, Appl. Phys. Lett. 72 (1998) 2165.
[9] R. Coustal, J. Chem. Phys. 38 (1958) 277.
[10] V. Dusastre, B. Omar, I.P. Parkin, G.A. Shaw, J. Chem. Soc., Dalton Trans. 19 (1997) 3505.
[11] R. Chen, D. Xu, G. Guo, L. Gui, J. Mater. Chem. 12 (2002) 2435.
[12] B. Li, Y. Xie, Y. Liu, J. Huang, Y. Qian, J. Solid State Chem. 158 (2001) 260.
[13] Y. Jiang, Y. Wu, Z. Yang, Y. Xie, Y. Qian, J. Cryst. Growth 224 (2001) 1.
[14] R. Harpeness, O. Palchik, A. Gedanken, V. Palchik, S. Amiel, M.A. Slifkin, A.M. Weiss, Chem. Mater. 14 (2002) 2094.
[15] J.J. Urban, D.V. Talapin, E.V. Shevchenko, C.R. Kagan, C.B. Murray, Nat. Mater. 6 (2007) 115.
[16] L. Mu, J. Wan, D. Ma, R. Zhang, W. Yu, Y. Qian, Chem. Lett. 34 (2005) 52.
[17] R. Chen, D. Xu, G. Guo, L. Gui, Electrochim. Acta 49 (2004) 2243.
[18] L. Zhang, Z. Ai, F. Jia, L. Liu, X. Hu, J.C. Yu, Chem. Eur. J. 12 (2006) 4185.
[19] G. Sáfrán, O. Geszti, G. Radnóczi, Vacuum 71 (2003) 299.
[20] B.C. Mohanty, S. Kasiviswanathan, Cryst. Res. Technol. 41 (2006) 59.
[21] J. Pola, Z. Bastl, J. Šubrt, A. Ouchi, Appl. Organomet. Chem. 14 (2000) 715.
[22] J. Pola, A. Ouchi, J. Org. Chem. 65 (2000) 2759.
[23] J. Pola, Z. Bastl, J. Šubrt, A. Ouchi, Appl. Organomet. Chem. 15 (2001) 924.
[24] J. Pola, D. Pokoná, J. Boháček, Z. Bastl, A. Ouchi, J. Anal. Appl. Pyrolysis 71 (2004) 739.
[25] A. Ouchi, K. Yamamoto, Y. Koga, J. Pola, J. Mater. Chem. 9 (1999) 563.
[26] A. Ouchi, Z. Bastl, J. Boháček, H. Orita, K. Miyazaki, S. Miyashita, P. Bezdička, J. Pola, Chem. Mater. 16 (2004) 3439.
[27] J.H. Scofield, J. Electron Spectrosc. Relat. Phenom. 8 (1976) 129.
[28] NIST Electron Inelastic-mean-free-paths Database, ver. 1.1, NIST Gaithersburg, MD, USA, 2000.
[29] J.L. Lábár, in: L. Frank, F. Ciampor (Eds.), Proceedings of the EUREM, vol. 12, Czechoslovak Society for Electron Microscopy, Brno, Czech Republic, 2000, p. 1379.
[30] JCPDS PDF-2 database, International Centre for Diffraction Data; Newton Square, PA, USA, release 2000.
[31] JCPDS PDF-2 database, International Centre for Diffraction Data; Newton Square, PA, USA, release 2004.
[32] D.H. Brown, R.J. Cross, D. Millington, J. Organomet. Chem. 125 (1977) 219.
[33] H.K. Spencer, M.P. Cava, J. Org. Chem. 42 (1977) 2937.
[34] W. Zhu, W. Wang, H. Xu, L. Zhou, L. Zhang, J. Shi, J. Cryst. Growth 295 (2006) 69.
[35] B. Zhou, J.-R. Zhang, L. Zhao, J.-M. Zhu, J.-J. Zhu, Ultrason. Sonochem. 13 (2006) 352.
[36] U.K. Gautam, C.N.R. Rao, J. Mater. Chem. 14 (2004) 2530.
[37] Z. Bastl, I. Spirovová, J. Horák, Solid State Ionics 95 (1997) 315.
[38] NIST X-ray Photoelectron Spectroscopy Database, version 3.4 (web version), http://srdata.nist.gov/xps/index.htm.
[39] I. Mishin, C. Herzig, Mater. Sci. Eng. A 260 (1999) 55.
[40] C. Kaito, A. Nonaka, S. Kimura, N. Suzuki, Y. Saito, J. Cryst. Growth 186 (1998) 386.
[41] W. Sitte, Solid State Ionics 94 (1997) 85.